

Shape-controlled TiO_2 nanomaterials-based hybrid solid-state electrolytes for solar energy conversion with a mesoporous carbon electrocatalyst

Lim, Seung Man; Moon, Juyoung; Baek, Uoon Chul; Lee, Jae Yeon; Chae, Youngjin; Park, Jung Tae

DOI

[10.3390/nano11040913](https://doi.org/10.3390/nano11040913)

Publication date

2021

Document Version

Final published version

Published in

Nanomaterials

Citation (APA)

Lim, S. M., Moon, J., Baek, U. C., Lee, J. Y., Chae, Y., & Park, J. T. (2021). Shape-controlled TiO_2 nanomaterials-based hybrid solid-state electrolytes for solar energy conversion with a mesoporous carbon electrocatalyst. *Nanomaterials*, 11(4), Article 913. <https://doi.org/10.3390/nano11040913>

Important note

To cite this publication, please use the final published version (if applicable). Please check the document version above.

Copyright

Other than for strictly personal use, it is not permitted to download, forward or distribute the text or part of it, without the consent of the author(s) and/or copyright holder(s), unless the work is under an open content license such as Creative Commons.

Takedown policy

Please contact us and provide details if you believe this document breaches copyrights. We will remove access to the work immediately and investigate your claim.



Article

Shape-Controlled TiO₂ Nanomaterials-Based Hybrid Solid-State Electrolytes for Solar Energy Conversion with a Mesoporous Carbon Electrocatalyst

Seung Man Lim ¹, Juyoung Moon ¹, Uoon Chul Baek ¹, Jae Yeon Lee ¹, Youngjin Chae ² and Jung Tae Park ^{1,*}

¹ Department of Chemical Engineering, Konkuk University, 120 Neungdong-ro, Gwangjin-gu, Seoul 05029, Korea

² Faculty of Industrial Design Engineering, Delft University of Technology, Landbergstraat 15, 2628 CE Delft, The Netherlands

* Correspondence: jtpark25@konkuk.ac.kr; Tel.: +82-2-450-3538; Fax: +82-2-450-3504

Abstract: One-dimensional (1D) titanium dioxide (TiO₂) is prepared by hydrothermal method and incorporated as nanofiller into a hybrid polymer matrix of polyethylene glycol (PEG) and employed as a solid-electrolyte in dye-sensitized solar cells (DSSCs). Mesoporous carbon electrocatalyst with a high surface area is obtained by the carbonization of the PVDC-g-POEM double comb copolymer. The 1D TiO₂ nanofiller is found to increase the photoelectrochemical performance. As a result, for the mesoporous carbon-based DSSCs, 1D TiO₂ hybrid solid-state electrolyte yielded the highest efficiencies, with 6.1% under 1 sun illumination, in comparison with the efficiencies of 3.9% for quasi solid-state electrolyte and 4.8% for commercial TiO₂ hybrid solid-state electrolyte, respectively. The excellent photovoltaic performance is attributed to the improved ion diffusion, scattering effect, effective path for redox couple transfer, and sufficient penetration of 1D TiO₂ hybrid solid-state electrolyte into the electrode, which results in improved light-harvesting, enhanced electron transport, decreased charge recombination, and decreased resistance at the electrode/electrolyte interface.

Keywords: solid-state electrolyte; titanium dioxide (TiO₂); one-dimensional (1D); photoelectrochemical; mesoporous carbon; dye-sensitized solar cell (DSSC)



Citation: Lim, S.M.; Moon, J.; Baek, U.C.; Lee, J.Y.; Chae, Y.; Park, J.T. Shape-Controlled TiO₂ Nanomaterials-Based Hybrid Solid-State Electrolytes for Solar Energy Conversion with a Mesoporous Carbon Electrocatalyst. *Nanomaterials* **2021**, *11*, 913. <https://doi.org/10.3390/nano11040913>

Academic Editor: Alexey Pestryakov

Received: 6 March 2021

Accepted: 31 March 2021

Published: 3 April 2021

Publisher's Note: MDPI stays neutral with regard to jurisdictional claims in published maps and institutional affiliations.



Copyright: © 2021 by the authors. Licensee MDPI, Basel, Switzerland. This article is an open access article distributed under the terms and conditions of the Creative Commons Attribution (CC BY) license (<https://creativecommons.org/licenses/by/4.0/>).

1. Introduction

Dye-sensitized solar cells (DSSCs) composed of mesoporous metal oxide-based photoanode, the precious-metal-based counter electrode, and liquid state electrolyte have attracted, over the last decade, considerable interest because of attractive characteristics such as high photoelectrochemical performance, low production cost, and ease of processing [1,2]. However, the liquid electrolyte-based DSSC has some drawbacks. Due to the leakage and volatilization of solvent, the photoelectrochemical performance of liquid electrolyte-based DSSC decreases with time, thereby suggesting that the electrolyte plays a key factor in improving the stability of DSSCs. An ideal electrolyte in DSSCs should have several advantages, such as thermal and chemical stability, a low absorption coefficient in the visible region, less leakage and volatilization, and high ion conductivity and diffusivity [3–6].

Several researchers have reported the use of poly(ethylene oxide) (PEO), poly(ethylene glycol) (PEG), and poly(methyl methacrylate) (PMMA) in DSSCs as quasi solid-state electrolytes [7–13]. The utilization of quasi solid-state electrolytes has many advantages, such as thermal and chemical stability and less leakage and evaporation of solvent. However, the photoelectrochemical performance of quasi solid-state electrolyte is lower than that of liquid state-electrolyte due to low ion diffusivity and poor permeability into mesoporous metal oxide based photoanode. Therefore, developing a quasi-solid-state or solid-state electrolyte with high conductivity and good interfacial contact with photoanode and counterelectrode is challenging.

The introduction of shape-controlled nanomaterials as nanofillers into the solid-state electrolyte is a simple and facile suggestion for improving photoelectrochemical performances, which reduces the crystallinity of the polymer main chain in the electrolyte and improves the ionic conductivity due to increased free volume for redox couple transport. In general, metal oxides such as WO_3 , SiO_2 , SnO_2 , and titanium dioxide (TiO_2), which are cost-effective and offer easy control of morphology, are utilized as nanofillers [14–22]. However, a quantitative comparison between one-dimensional (1D) TiO_2 and commercial TiO_2 -based solid electrolytes in photoelectrochemical applications has not been conducted often because it is difficult to control the shape and size of nanomaterials.

Meanwhile, earth abundant mesoporous carbon materials present a great potential replacement of precious-metal-based counter electrode because of their high electrocatalytic activity, good electrochemical stability, and large surface area for rapid interface reactions [23,24]. In this regard, it is reported to be possible to directly prepare mesoporous carbon nanostructure by self-assembling a block copolymer as carbon precursors [25]. However, double comb copolymer-derived mesoporous carbon counterelectrodes for DSSCs based on quasi solid-state or solid-state electrolytes are still in their infancy. Therefore, a systematic study is needed to clarify how a mesoporous carbon electrocatalyst and the shape-controlled nanomaterials based solid-state electrolyte impact on electrochemical and optical properties and their impact on the performance of photovoltaic devices.

In this study, the effect of the shape-controlled TiO_2 nanomaterials in the hybrid solid-state electrolytes on the photoelectrochemical characteristics of mesoporous carbon-based DSSCs was investigated systematically. A mesoporous carbon electrocatalyst with a high surface area is obtained by the carbonization of the PVDC-g-POEM double comb copolymer. A nanofiller material in the form of 1D TiO_2 was added to the hybrid solid-state electrolyte to enhance the ion diffusion, scattering effect, redox couple transfer, and penetration of electrolyte into the electrode, therefore improving the photochemical performance of the mesoporous carbon-based DSSCs. This research provides an essential first step toward the use of hybrid solid-state electrolytes containing shape-controlled TiO_2 nanomaterials in mesoporous carbon-based photoelectrochemical applications.

2. Experimental Section

2.1. Materials

In this study, the chemicals were used as obtained, i.e., no further purification was conducted. Titanium (IV) butoxide (TTBT, 97%), HCl (37 wt%), I_2 , LiI, titanium diisopropoxide bis(ethylacetoacetate), 1-methyl-3-propylimidazolium iodide (MPII), PEG ($M_w = 10,000 \text{ g mol}^{-1}$), and H_2PtCl_6 were purchased from Sigma-Aldrich (St. Louis, MO, USA). Acetonitrile, 2-propanol, and chloroform were purchased from J. T. Baker (Thermo Fisher Scientific, Waltham, MA, USA). Deionized water ($>18 \text{ M}\Omega\text{m}$) was obtained with a water purification system made by MilliporeSigma (Burlington, MA, USA). Commercial TiO_2 paste (Ti-Nanoxide, D20) and ruthenium dye (N719) were purchased from Solaronix SA (Aubonne, Switzerland). Commercial TiO_2 powder (P25) was prepared by Evonik Industries AG (formerly Degussa, Essen, Germany). Fluorine-doped tin oxide (FTO, TEC-7) conducting substrate was purchased from Pilkington, France.

2.2. Preparation of 1D TiO_2 Hybrid Solid-State Electrolyte

The one-dimensional TiO_2 nanorod (1D TiO_2) deposited onto FTO substrate was synthesized via hydrothermal method [26]. First, 0.8 mL of titanium (IV) butoxide (TTBT) was added into 60 mL of 6 M HCl solution. FTO substrate ($3 \times 4 \text{ cm}$) was cleaned with chloroform and 2-propanol and placed in a Teflon-lined autoclave, wherein the conductive side of the FTO was placed face down. Then, the TTBT/HCl solution was transferred into the Teflon-lined autoclave followed by heating at $150 \text{ }^\circ\text{C}$ for 6 h. After reaction, 1D TiO_2 deposited-FTO substrate was cleaned with water and ethanol several times and dried at $50 \text{ }^\circ\text{C}$ for 30 min. Then, 1D TiO_2 were physically scrapped off from the 1D TiO_2 deposited-FTO substrate with a slide glass. 1D TiO_2 hybrid solid-state electrolyte were prepared

with 1g of PEG, 0.15 g of LiI, 0.15g of 0.03 g of MPPII, and 10 mL of I2 in acetonitrile with the addition of the 0.09 g of 1D TiO₂ prepared in this study. It should be noted that 1D TiO₂ nanomaterials in the solid-state electrolyte were well dispersed due to the plentiful amount of hydroxyl group of metal oxides. In addition, quasi solid-state electrolytes were prepared according to a previous report as control samples [27]. And commercial TiO₂ hybrid solid-state electrolytes were prepared from PEG-based electrolyte with commercial TiO₂ as a control.

2.3. Preparation of Mesoporous Carbon Electrocatalyst Based Counterelectrode

The mesoporous carbon electrocatalyst-based counter electrode was prepared by depositing on the prepared FTO substrate according to the modified protocol previously reported by our group [28]. In brief, 0.05 g of PVDC-*g*-POEM double comb copolymer was first dissolved in 1.5 mL of THF. Separately, 0.15 mL of concentrated HCl (37 wt%) was slowly added to 0.15 mL of deionized water at room temperature under stirring speed of 500 rpm. After aging for 15 min at room temperature, the HCl/H₂O solution was slowly added to the PVDC-*g*-POEM double comb copolymer solution with a stirring speed of 300 rpm, followed by annealing at 60 °C for 1h to obtain a viscous solution. Then, the viscous PVDC-*g*-POEM double comb copolymer solution was screen-printed on the FTO substrate, and the printed film was calcinated at 550 °C in Ar for 30 min.

2.4. Preparation of 1D TiO₂ Hybrid Solid-State Electrolyte Based DSSCs

The FTO substrate was cleaned with chloroform and 2-propanol. As a photoanode, the cleaned FTO conductive side was spin coated with 1 wt% titanium diisopropoxide bis(ethylacetoacetate) 2-butanol solution followed by calcination at 450 °C for 30 min. To prepare nanocrystalline TiO₂, commercial TiO₂ paste (Ti-Nanoxide, D20) was deposited on the prepared FTO substrate using the doctor-blade method and dried at 50 and 80 °C for 1 h, respectively, followed by sintering at 450 °C for 30 min. Then, the prepared photoanode was immersed in 0.1 mM N719 dye ethanol solution at 50 °C for 3 h. According to a previously reported procedure, DSSCs with an active area of 0.4 cm² were constructed by drop-casting of 1D TiO₂ hybrid solid-state electrolyte solution onto the photoanode and covering with the counterelectrode [29]. And then, the DSSCs were dried in a drying oven at 50 °C for 24 h for solvent evaporation.

2.5. Characterization

The surface and cross-sectional morphologies were acquired by field emission scanning electron microscopy (FE-SEM) (SU8010, Hitachi, Tokyo, Japan). Transmission electron microscope (TEM) images were obtained from a Philips CM30 microscope operating at 300 kV to observe nanostructures of samples (Philips CM30, Amsterdam, The Netherlands). The crystalline structure of 1D TiO₂ was obtained by X-ray diffraction (XRD) spectroscopy (Smartlab, Rigaku, Tokyo, Japan) with CuK α radiation ($\lambda = 1.5406 \text{ \AA}$). The specific surface area and pore volume of the mesoporous carbon were measured using the N₂ adsorption-desorption isotherm via the Brunauer-Emmett-Teller (BET) methods. Before the adsorption-desorption measurement, the mesoporous carbon was degassed at 70 °C under a dynamic vacuum (10^{-2} Torr) for 1 h. Intensity-modulated photocurrent/voltage spectroscopy (IMPS/IMVS) was used to investigate electron diffusion and recombination properties. UV-vis diffuse-reflectance spectra were characterized by spectrophotometry (Mega-900, Scinco, Seoul, Korea). Thickness of photoanode and counterelectrode was measured using an alpha-step IQ surface profile (KLA Tencor). The current density–voltage (*J*–*V*) measurements were performed using a potentiostat (Compactstat.h, Ivium Technologies, Eindhoven, The Netherlands). The solar simulator equipped with a 1000 W xenon lamp was used as light source (SunLite, Abet Technologies, Inc., Milford, CT, USA). Electrochemical impedance spectroscopy (EIS) characteristics were measured by a potentiostat under open-circuit voltage in a frequency range of 0.01–100 kHz. Incident photo-to-electron conversion efficiency (IPCE) spectra were obtained by IPCE system (IPCEPEIPCE100S,

HS Technologies, Plano, TX, USA). The photovoltaic parameters were calculated using Equations (1) and (2):

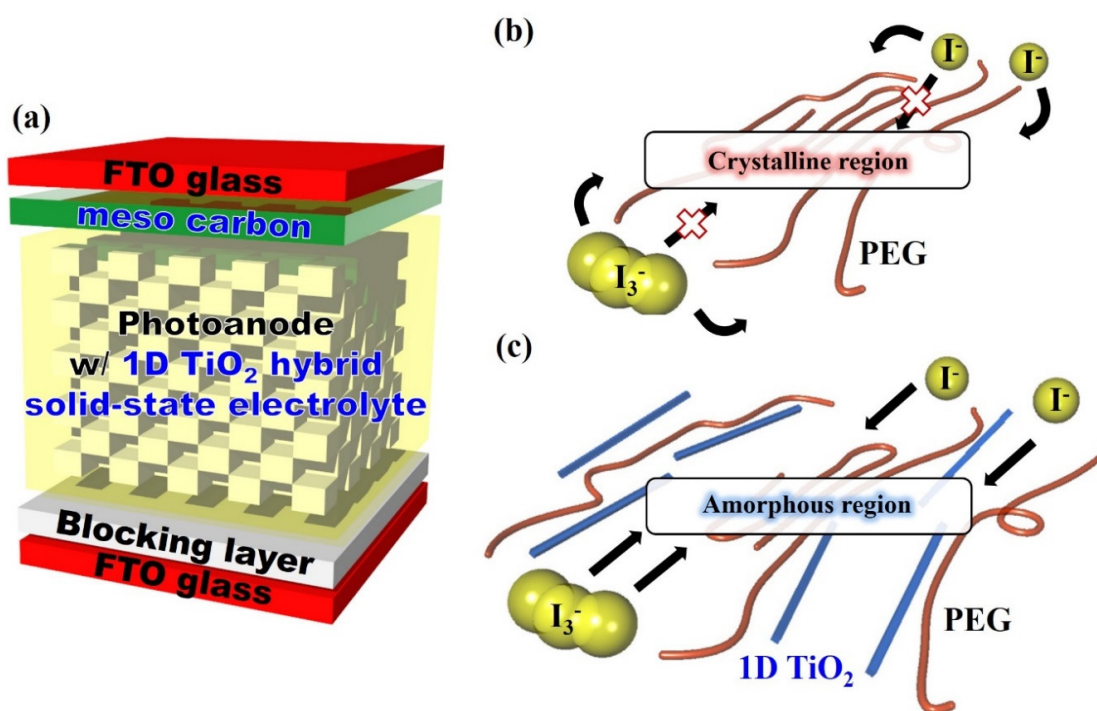
$$FF = V_{max} \times J_{max} / V_{oc} \times J_{sc} \quad (1)$$

$$\eta = V_{max} \times J_{max} / P_{in} \times 100 = V_{oc} \times J_{sc} \times FF / P_{in} \times 100 \quad (2)$$

where η is the photovoltaic conversion efficiency, J_{sc} is short-circuit current density, V_{oc} is the open-circuit voltage, P_{in} is incident light power, FF is fill factor, and J_{max} and V_{max} are current density and voltage, respectively, when maximum power is achieved.

3. Results and Discussion

The schematic of the dye-sensitized solar cells (DSSCs) fabricated in this study and the possible redox couple reaction in two types of electrolytes are shown in Scheme 1. In quasi-solid-state electrolytes, the redox couple transfers in several ways, such as polymer segment motion or ion diffusion. However, redox couple transfer is restricted by high crystallinity of the PEG crystalline region of quasi-solid-state electrolyte, resulting in low ionic conductivity. Therefore, reducing the crystallinity of the polymer main chain is a key factor for improving the photoelectrochemical performance of DSSCs [30,31]. The hydrophilic 1D TiO₂ interacted with the PEG main chain in the 1D TiO₂ hybrid solid-state electrolyte, resulting in an amorphous region, which created free volume from the crystalline region. This amorphous region could be an effective path for redox couple transfer, thereby resulting in enhanced ionic conductivity.



Scheme 1. (a) Schematic of the dye-sensitized solar cells (DSSCs) fabricated in this study and the possible redox couple reaction of (b) quasi solid-state electrolyte and (c) One-dimensional (1D) titanium dioxide (TiO₂) hybrid solid-state electrolyte.

The SEM and TEM images of 1D TiO₂ and commercial TiO₂ are shown in Figure 1. The surface of the FTO was homogeneously covered with vertically aligned 1D TiO₂ with lengths of 3 μm and diameters of 250 nm, as shown in Figure 1a,b. It should be noted that the crystalline phase of the FTO substrate was similar to that of 1D TiO₂; the 1D TiO₂ nanostructure was grown on FTO without the Ti seed layer [32]. Figure 1c shows the TEM image of a 1D TiO₂ with a diameter of about 250 nm, which is consistent with the SEM images. Moreover, the commercial TiO₂ agglomerated to some degree with 30 nm in size, as shown in Figure 1d. Note that Figure S1 shows the size distribution of commercial TiO₂

and 1D TiO₂. The average diameter of the commercial TiO₂ was approximately 20~30 nm. The diameter of the 1D TiO₂ was approximately 240~250 nm.

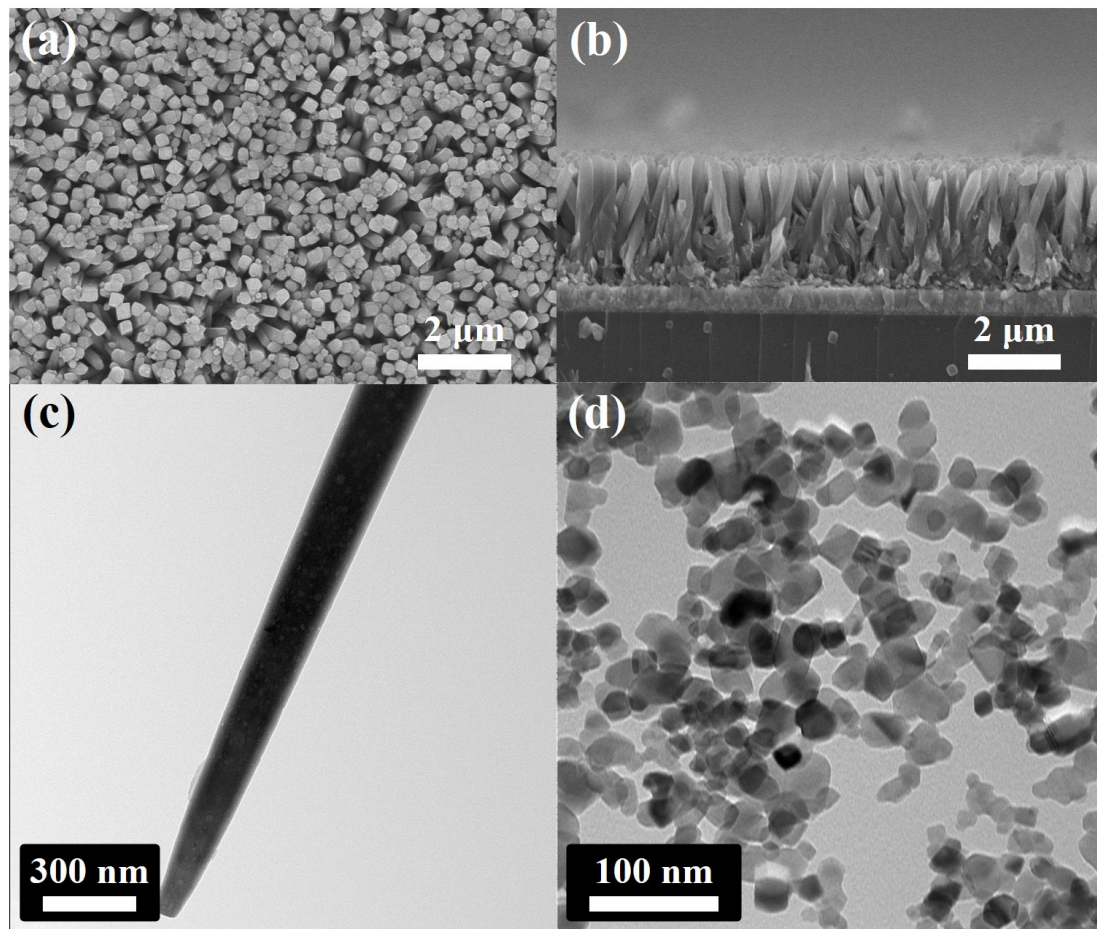


Figure 1. Field emission scanning electron microscopy (FE-SEM) images of vertically aligned 1D TiO₂ grown on Fluorine-doped tin oxide (FTO) glass via the hydrothermal process: (a) top-view and (b) cross-section of 1D TiO₂. Transmission electron microscope (TEM) image of (c) 1D TiO₂ and (d) commercial TiO₂.

Figure 2 shows the XRD pattern of the as-prepared 1D TiO₂ and commercial TiO₂. 1D TiO₂ showed several sharp peaks at 2 theta values of 27.5°, 36.2°, 38.4°, 41.4°, 44.4°, 54.5°, and 56.6°, corresponding to (110), (101), (200), (111), (210), (211), and (220) crystal planes of the rutile TiO₂ phase, respectively (ICDD-JCPDS database, no. 77-0441). The commercial TiO₂ exhibited several sharp peaks centered at 2 theta values of 25.5°, 38.0°, 48.2°, 54.3°, and 55.2°, which correspond to the (101), (004), (200), (105), and (211) reflections, respectively, of the anatase form of TiO₂ (JCPDS no. 21-1272). These results indicate the successful preparation of highly crystalline 1D TiO₂ from the TiO₂ metal oxide precursor using the hydrothermal process. According to the Mie theory, the superior scattering center is found in those with sizes comparable to the wavelength of light, and the light scattering occurs due to higher incidence of light trapping in photovoltaic devices [33]. Therefore, we can expect that high-aspect-ratio materials such as 1D TiO₂ in rutile phase give rise to an improved light scattering effect compared to low-aspect-ratio materials such as commercial TiO₂ in anatase phase, leading to enhanced photovoltaic performance. Moreover, replacing our suggested rutile phase of 1D TiO₂ with commercial rutile phase TiO₂ as a nanofiller is expected to vary the photoelectrochemical characteristics, which are currently investigated in our lab.

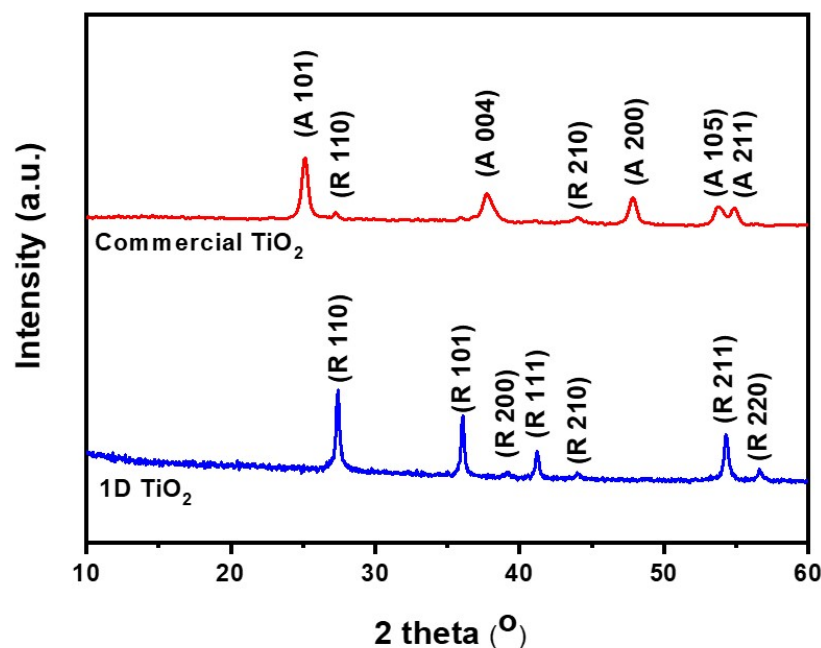


Figure 2. X-ray diffraction (XRD) patterns of 1D TiO₂ and commercial TiO₂ where R and A denote rutile and anatase phases, respectively.

Interfacial contact between the photoanode and the electrolyte is of importance in determining the photoelectrochemical performance of DSSCs. Therefore, the top-view SEM images of the photoanode were taken before and after casting (quasi) solid-state electrolytes, as shown in Figure 3. Before electrolyte casting, the metal oxide nanoparticles had a size of 30 nm in photoanode, and the pores between the structures were detectable, as shown in Figure 3a. Figure 3b presents a SEM image for a top-view of a quasi-solid-state electrolyte filled mesoporous photoanode. The quasi-solid-state electrolyte uniformly covered the mesoporous photoanode without any noticeable defective sites. Figure 3c,d presents an SEM image for a top-view of the mesoporous photoanode with commercial TiO₂ hybrid solid-state electrolyte and 1D TiO₂ hybrid solid-state electrolyte, respectively. The commercial TiO₂ maintains the morphological structure in the polymer matrix, showing a nanoscale range. Moreover, the 1D TiO₂ in the 1D TiO₂ hybrid solid-state electrolyte indicates that the 1D TiO₂ plays a role as an effective light scattering center. It should be noted that commercial TiO₂ or 1D TiO₂ nanomaterials lead to the enhanced interaction between electrolyte and photoanode, resulting in PEG-based electrolyte remaining in solids and behaving as highly viscous liquids. In addition, the thickness of photoanodes was increased from 7 to 10 μm after commercial TiO₂ and 1D TiO₂ hybrid solid-state electrolyte casting.

The electron transport properties of 1D TiO₂ hybrid solid-state electrolyte, including diffusion coefficient (D_n), electron lifetime (τ_r), electron diffusion length (L_n), and electron collection efficiency (η_{cc}) as a function of J_{sc} were characterized using IMPS/IMVS analysis, as shown in Figure 4. IMPS/IMVS analyses are useful for obtaining electron transport time (τ_t) and electron lifetime (τ_r). Then, the electron transport time was converted to diffusion coefficient (D_n) as follows:

$$D_n = d^2 / 2.35 \tau_t \quad (3)$$

where d is the film thickness of photoanode. In addition, electron diffusion length (L_n), and electron collection efficiency (η_{cc}) were obtained as follows:

$$L_n = (D_n \tau_r)^{0.5} \quad (4)$$

$$\eta_{cc} = 1 - \tau_t / \tau_r \quad (5)$$

where τ_r and τ_t values are obtained using IMVS and IMPS analysis, respectively [34,35]. The D_n and τ_r values of DSSCs based on 1D TiO₂ hybrid solid-state electrolyte were higher than that of quasi solid-state electrolyte and commercial TiO₂ hybrid solid-state electrolyte, indicating that the introduction of 1D TiO₂ as nanofiller in electrolyte is a good suggestion to enhance electron transfer of photoelectrochemical devices. The L_n and η_{cc} values of the 1D TiO₂ hybrid solid-state electrolyte are higher than those of the quasi solid-state electrolyte for the entire range of J_{sc} . This demonstrates that it is the amorphous region of 1D TiO₂ hybrid solid-state electrolyte which is responsible for enhanced charge transport and reduced recombination in the photoelectrochemical devices. It should be noted that the 1D TiO₂ hybrid solid-state electrolyte provides a more effective path for redox couple transfer than commercial TiO₂ hybrid solid-state electrolyte due to the facile formation of an amorphous region.

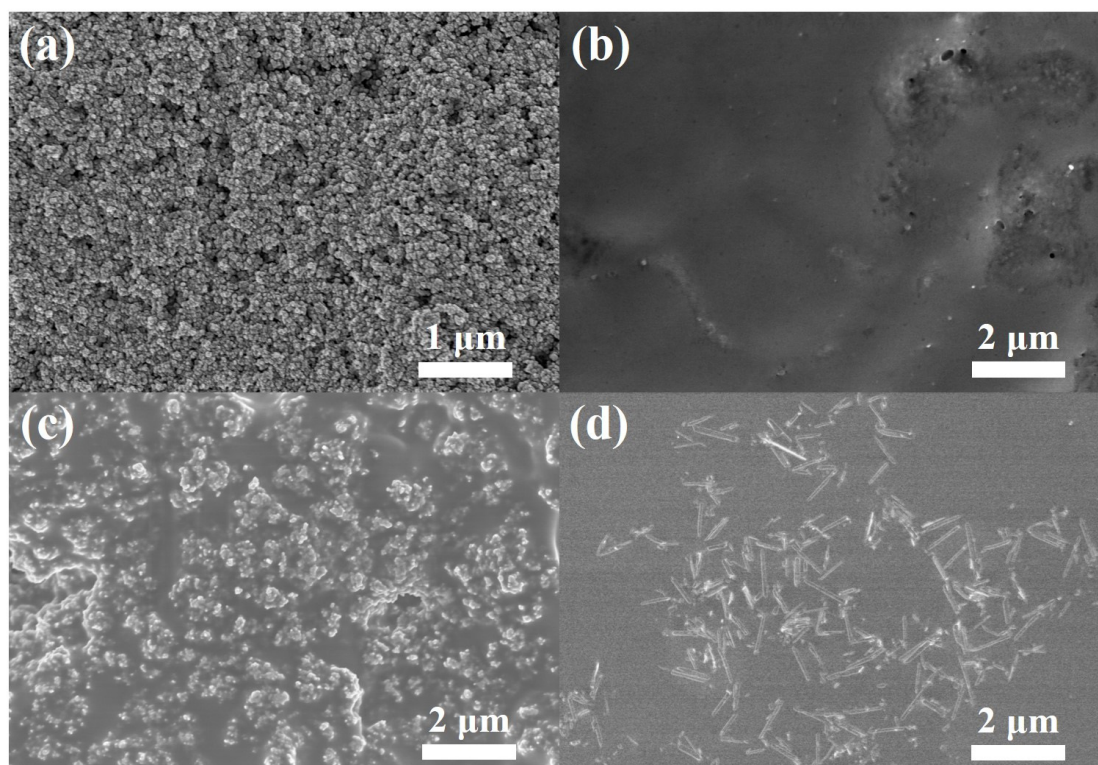


Figure 3. SEM image of the (a) photoanode, (b) photoanode after quasi solid-state electrolyte casting, (c) photoanode after commercial TiO₂ hybrid solid-state electrolyte casting and (d) photoanode after 1D TiO₂ hybrid solid-state electrolyte casting.

To investigate the scattering effect of 1D TiO₂ hybrid solid-state electrolyte, diffuse reflectance of DSSCs fabricated with symmetric photoanodes was characterized, as shown in Figure 5. In the short wavelength region, i.e., 300–450 nm, there was no difference in the diffuse reflectance between the quasi solid-state electrolyte and two types of hybrid solid-state electrolytes. However, in the wavelength region of 450–600 nm, the 1D TiO₂ hybrid solid-state electrolyte had higher diffuse reflectance than the quasi solid-state electrolyte and commercial TiO₂ hybrid solid-state electrolyte, suggesting that the use of 1D TiO₂ induced scattering effect, which resulted in higher light-harvesting properties. It should be noted that the adding of a high-aspect-ratio nanomaterial is an effective method for enhancing the light scattering capacity of photovoltaic devices, which increases an equivalent optical path and thereby enhances a photocurrent density [14]. Moreover, replacing our suggested 1D TiO₂ with different aspect ratio nanomaterials or large particles as a nanofiller is expected to improve the light scattering property, which is currently being investigated in our lab.

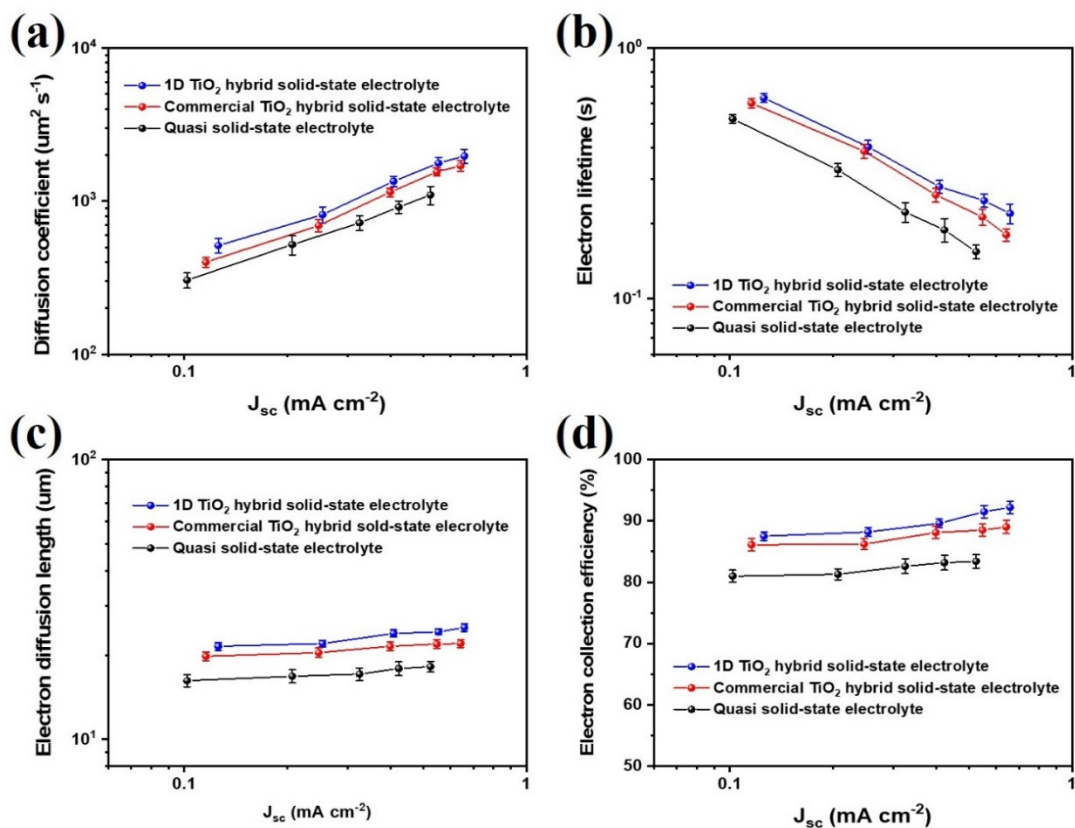


Figure 4. (a) Diffusion coefficients (D_n), (b) recombination time (τ_r), (c) electron diffusion length (L_n), and (d) electron collection efficiency (η_{cc}) as functions of the J_{sc} for the mesoporous carbon-based dye-sensitized solar cells (DSSCs) with quasi solid-state electrolyte, commercial TiO_2 hybrid solid-state electrolyte and 1D TiO_2 hybrid solid-state electrolyte measured by IMPS and IMVS. Error bars represent the standard deviation of at least 5 cells.

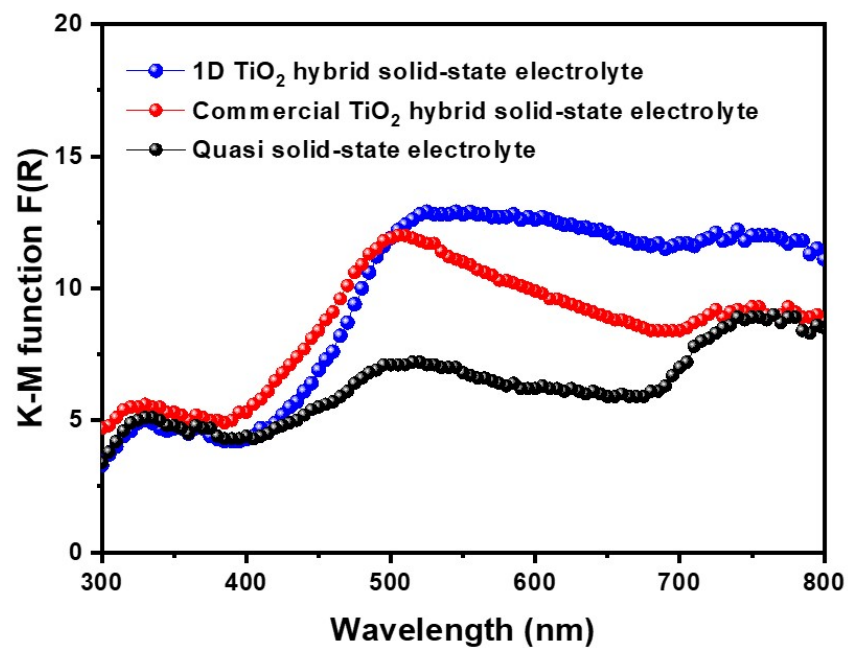


Figure 5. Kubelka-Munk (KM) function of quasi solid-state electrolyte, commercial TiO_2 hybrid solid-state electrolyte, and 1D TiO_2 hybrid solid-state electrolyte.

To investigate the photovoltaic properties of mesoporous carbon-based DSSCs with 1D TiO₂ hybrid solid-state electrolytes, the current density-voltage (*J-V*) measurement curves are shown in Figure 6a. The photovoltaic parameters, short-circuit current density (*J_{sc}*), open-circuit voltage (*V_{oc}*), *FF*, and overall energy conversion efficiency (*η*) are listed in Table 1. It should be noted that the mesoporous carbon derived from PVDC-*g*-POEM double comb copolymer showed the BET surface area of 472.15 m²/g and highly ordered porosity, as results in one of the best counterelectrode materials for photoelectrochemical devices. (Figure S2) [28] For reliability, we additionally provide photovoltaic parameters of the different sets of mesoporous carbon-based DSSCs with 1D TiO₂ hybrid solid-state electrolytes. The photovoltaic parameters with error bars of the standard deviations for at least five cells were summarized in Figure S3 and Table S1. For a mesoporous carbon-based DSSCs, using a quasi-solid-state electrolyte, *J_{sc}* and *V_{oc}* are 10.7 mA cm⁻² and 0.60 V, respectively, whereas the *FF* and the *η* are 0.59 and 3.9%, respectively. In comparison, the solar conversion efficiency of the 1D TiO₂ hybrid solid-state electrolyte was the highest achieved in this research (6.1%); this correlates with the highest *J_{sc}* of 14.6 mA cm⁻², a *V_{oc}* of 0.65 V, and a *FF* of 0.64. It should be noted that the efficiency of the mesoporous carbon-based DSSCs using the 1D TiO₂ hybrid solid-state electrolyte represents one of the highest values reported for Pt-free counterelectrode-based DSSCs to date, as shown in Table S2 [36–40]. Moreover, the carbon-based DSSCs fabricated with commercial TiO₂ hybrid solid-state electrolyte show efficiency of 4.8% with a *J_{sc}*, *V_{oc}*, and *FF* of 12.7 mA cm⁻², 0.63 V, and 0.60, respectively. The mesoporous carbon-based DSSCs with 1D TiO₂ hybrid solid-state electrolyte achieved more than 30% *J_{sc}* value compared to the quasi solid-state electrolyte, demonstrating that the introduction of 1D TiO₂ to electrolyte enhanced ion diffusion of the redox couple as well as the scattering effect, thereby improving the light-harvesting. In addition, a slightly higher *V_{oc}* value was observed in mesoporous carbon-based DSSCs with 1D TiO₂ hybrid solid-state electrolyte. Moreover, the *V_{oc}* value can be obtained as follows:

$$V_{oc} = |V_{fb} - V_{red}| \quad (6)$$

where *V_{fb}* is the Fermi level potential of photoanode and *V_{red}* is the reduction potential of redox couple in electrolyte [41]. Possible contributions to the enhanced *V_{oc}* value include the decreased charge recombination, electron back reaction loss, and the reduction of the *V_{red}* of the electrolyte by the 1D TiO₂. The decreasing of the charge recombination and electron back reaction loss in mesoporous carbon-based DSSCs with 1D TiO₂ hybrid solid-state electrolyte were also characterized using previous IMPS/IMVS measurements. The Nyquist plots and equivalent circuit diagram of the mesoporous carbon-based DSSCs with 1D TiO₂ hybrid solid-state electrolyte are shown in Figure 6b,c, respectively. The electrochemical parameters of mesoporous carbon-based DSSCs are listed in Table 2. An equivalent circuit model consisted of the series resistance (*R_s*), which is ohmic resistance of the FTO substrate, counterelectrode/electrolyte interfacial charge transfer resistance (*R₁*), photoanode/electrolyte interfacial charge transfer resistance (*R₂*), and Warburg diffusion resistance (*W_s*). Upon analysis of Nyquist impedance data through fitting with the equivalent circuit, the total resistance values of mesoporous carbon-based DSSCs with 1D TiO₂ hybrid solid-state electrolyte were significantly reduced compared to the quasi solid-state electrolyte. This phenomenon may be explained by the increased electron transport in mesoporous carbon-based DSSCs with 1D TiO₂ hybrid solid-state electrolyte, leading to decreased resistance at the photoanode/electrolyte interface. Incident photon-to-electron conversion efficiency (IPCE) quantifies the internal quantum and light-harvesting efficiencies at an incident wavelength for DSSCs. Figure 6d presents the IPCE spectra for mesoporous carbon-based DSSCs with the 1D TiO₂ hybrid solid-state electrolyte. The DSSCs based on the 1D TiO₂ hybrid solid-state electrolyte showed the maximum IPCE of about 80%, while the DSSCs based on the quasi solid-state electrolyte exhibited the maximum IPCE of about 60%. Furthermore, the *J_{sc}* values from the IPCE curves were quite consistent with those determined from *J-V* curves for all of the mesoporous carbon-based DSSCs, as shown in Table 1. The enhanced IPCE value of the mesoporous carbon-based

DSSCs with the 1D TiO₂ hybrid solid-state electrolyte was attributed to enhanced light harvesting efficiency, consistent with the previous diffuse reflectance. Furthermore, Figure 6e showed the stability behaviors of the mesoporous carbon-based DSSCs with the 1D TiO₂ hybrid solid-state electrolyte. After 10 days, the cell efficiency of its devices remained stable, suggesting that the mesoporous carbon and 1D TiO₂ hybrid solid-state electrolyte have good electrochemical stability and enhanced electrode/electrolyte interface. Moreover, it should be noted that the cell efficiency of quasi solid-state electrolyte and commercial TiO₂ hybrid solid-state electrolyte is lower than that of 1D TiO₂ hybrid solid-state electrolyte after stability testing.

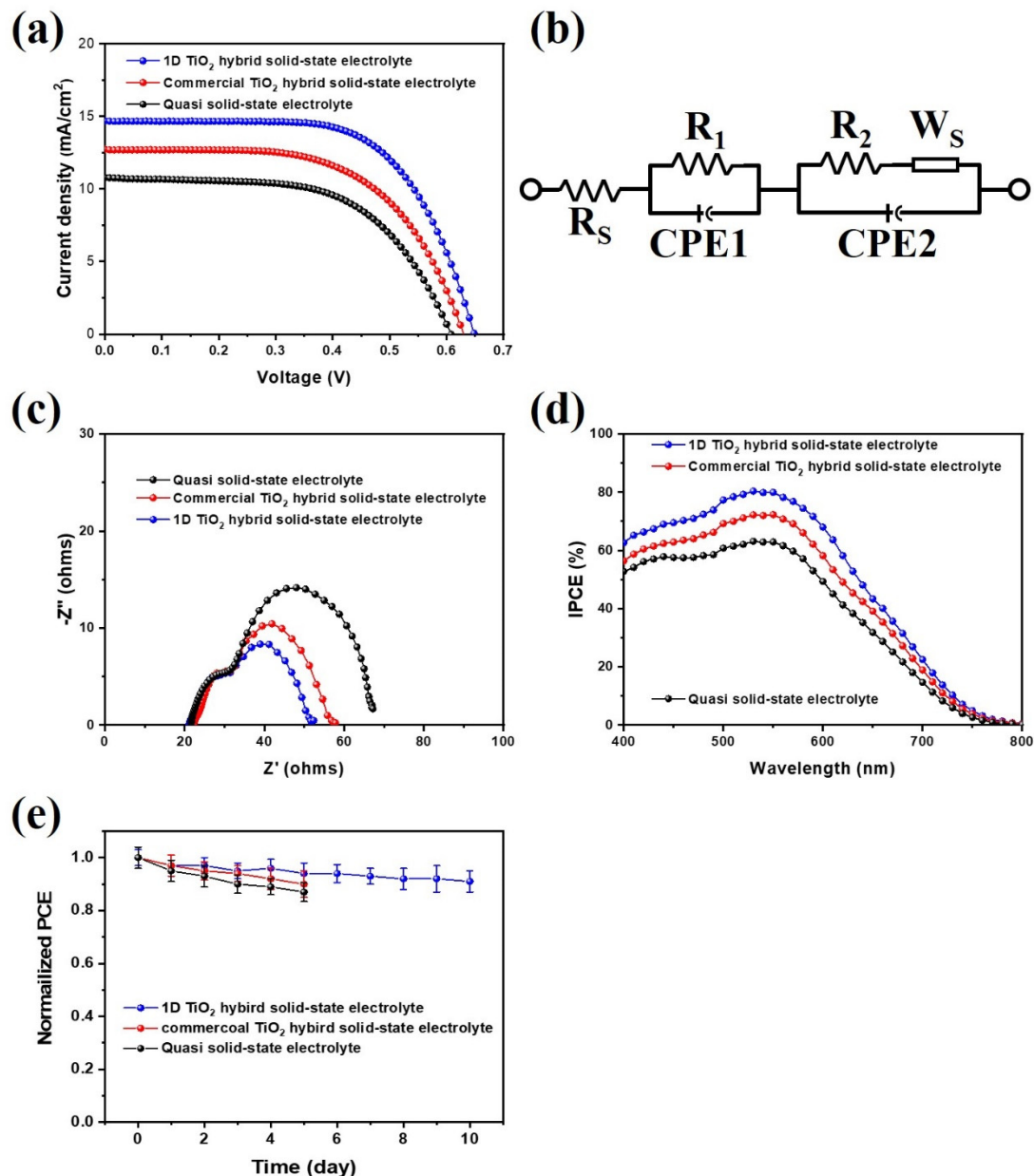


Figure 6. (a) *J*-*V* curves, (b) equivalent circuit diagram, (c) Electrochemical impedance spectroscopy (EIS) Nyquist plots, and (d) Incident photo-to-electron conversion efficiency (IPCE) curves of mesoporous carbon-based DSSCs fabricated with quasi solid-state electrolyte, commercial TiO₂ hybrid solid-state electrolyte, and 1D TiO₂ hybrid solid-state electrolyte at 100 mW/cm². (e) Normalized cell efficiency of the mesoporous carbon-based DSSCs with 1D TiO₂ hybrid solid-state electrolyte (40–50% relative humidity). Error bars represent the standard deviation of at least 5 cells.

Table 1. Photovoltaic properties of mesoporous carbon-based dye-sensitized solar cells (DSSCs) with quasi solid-state electrolyte, commercial TiO₂ hybrid solid-state electrolyte, and 1D TiO₂ hybrid solid-state electrolyte at 100 mW/cm² (AM 1.5) ^{a, b, c, d, e, f, g, h, i}.

Electrolyte	V _{oc} (V)	J _{sc} ^g (mA/cm ²)	J _{sc} ^h (mA/cm ²)	FF	η (%)
Quasi solid-state electrolyte	0.60 ± 0.04	10.7 ± 0.7	10.3	0.59 ± 0.02	3.9 ± 0.20
Commercial TiO ₂ hybrid solid-state electrolyte	0.63 ± 0.04	12.7 ± 0.4	12.0	0.60 ± 0.01	4.8 ± 0.15
1D TiO ₂ hybrid solid-state electrolyte	0.65 ± 0.03	14.6 ± 0.6	13.8	0.64 ± 0.03	6.1 ± 0.20

^a Quasi solid-state electrolyte consists of PEG, LiI, MPIL, and I₂ in acetonitrile. ^b Commercial TiO₂ hybrid solid-state electrolyte consist of commercial TiO₂, PEG, LiI, MPIL, and I₂ in acetonitrile. ^c 1D TiO₂ hybrid solid-state electrolyte consist of 1D TiO₂, PEG, LiI, MPIL, and I₂ in acetonitrile. ^d The photoactive area for DSSCs was 0.16 cm². ^e The thickness of the photoanode was approximately 7 μm. ^f The thickness of the counterelectrode was approximately 5 μm. ^g Determined from *J-V* curves. ^h Determined from IPCE curves. ⁱ Error bars represent the standard deviation of at least 5 cells.

Table 2. Electrochemical parameters of mesoporous carbon-based DSSCs with quasi solid-state electrolyte, commercial TiO₂ hybrid solid-state electrolyte and 1D TiO₂ hybrid solid-state electrolyte, as determined by EIS analysis at 100 mW/cm² (AM 1.5). Error bars represent the standard deviation of at least 5 cells.

Electrolyte	R _s (Ω)	R ₁ (Ω)	R ₂ (Ω)	W _s (Ω)
Quasi solid-state electrolyte	21.6 ± 3.5	9.8 ± 1.5	34.4 ± 5.0	2.4 ± 0.3
Commercial TiO ₂ Hybrid solid-state electrolyte	22.3 ± 3.0	8.7 ± 1.2	25.5 ± 4.5	2.0 ± 0.3
1D TiO ₂ Hybrid solid-state electrolyte	21.1 ± 3.5	9.6 ± 1.5	20.1 ± 4.0	1.8 ± 0.2

4. Conclusions

1D TiO₂ was prepared by hydrothermal method and used as a nanofiller in a PEG-based hybrid solid-state electrolyte to enhance the ion diffusion, scattering effect, effective path for redox couple transfer, and sufficient penetration of hybrid solid-state electrolyte into the electrode, thereby improving the photoelectrochemical performance of mesoporous carbon-based DSSCs. Mesoporous carbon electrocatalyst was prepared using a carbonization approach with PVDC-*g*-POEM double comb copolymers. The mesoporous carbon-based DSSCs based on 1D TiO₂ hybrid solid-state electrolyte (6.1%) showed a higher cell performance than those with quasi solid-state electrolyte (4.8%) and commercial TiO₂ hybrid solid-state electrolyte (3.9%). These results indicate that the addition of a 1D TiO₂ nanofiller to a hybrid solid-state electrolyte improves the light-harvesting and charge transport, reduces recombination, and decreases the resistance at the electrode/electrolyte interface. We believe this suggestion presents a promising way to prepare hybrid solid-state electrolytes with enhanced performance for mesoporous carbon-based photoelectrochemical applications.

Supplementary Materials: The following are available online at <https://www.mdpi.com/article/10.3390/nano11040913/s1>, Figure S1: The size distribution of commercial TiO₂ (a) and 1D TiO₂ (b). Figure S2: (a) N₂ adsorption (filled symbols) and desorption (unfilled symbols) isotherms of mesoporous carbon electrocatalyst derived from PVDC-*g*-POEM double comb copolymer and (b) SEM of mesoporous carbon electrocatalyst. Figure S3: Photovoltaic parameters of mesoporous carbon-based DSSCs fabricated with quasi solid-state electrolyte, commercial TiO₂ hybrid solid-state electrolyte and 1D TiO₂ hybrid solid-state electrolyte at 100 mW/cm². Error bars represent the standard deviation of at least 5 cells. Table S1: Photovoltaic parameters of mesoporous carbon-based dye-sensitized solar cells (DSSCs) with quasi solid-state electrolyte, commercial TiO₂ hybrid solid-state electrolyte, and 1D TiO₂ hybrid solid-state electrolyte at 100 mW/cm² (AM 1.5). Table S2: Comparison of photovoltaic parameters of Pt-free counterelectrode based DSSCs fabricated with solid-state electrolytes reported in the literature.

Author Contributions: Conceptualization, S.M.L.; formal analysis, J.M.; investigation, U.C.B., J.Y.L., and Y.C.; writing—review and editing, J.T.P. All authors have read and agreed to the published version of the manuscript.

Funding: This paper was supported by Konkuk University in 2017.

Institutional Review Board Statement: Not applicable. This study was not involved on humans or animals.

Informed Consent Statement: Not applicable. This study was not provided on the humans.

Data Availability Statement: No data available.

Conflicts of Interest: The authors declare no conflict of interest.

References

1. Chu, S.; Majumdar, A. Opportunities and challenges for a sustainable energy future. *Nature* **2012**, *488*, 294. [[CrossRef](#)] [[PubMed](#)]
2. O'Regan, B.; Grätzel, M. A low-cost, high-efficiency solar cell based on dye-sensitized colloidal TiO₂ films. *Nature* **1991**, *353*, 737. [[CrossRef](#)]
3. Gong, J.; Sumathy, K.; Qiao, Q.; Zhou, Z. Review on dye-sensitized solar cells (DSSCs): Advanced techniques and research trends. *Renew. Sust. Energ. Rev.* **2017**, *68*, 234. [[CrossRef](#)]
4. Li, B.; Wang, L.; Kang, B.; Wang, P.; Qiu, Y. Review of recent progress in solid-state dye-sensitized solar cells. *Sol. Energy Mater. Sol. Cells* **2006**, *90*, 549. [[CrossRef](#)]
5. Venkatesan, S.; Lee, Y.-L. Nanofillers in the electrolytes of dye-sensitized solar cells—A short review. *Coord. Chem. Rev.* **2017**, *353*, 58. [[CrossRef](#)]
6. Kim, J.H.; Kang, M.-S.; Kim, Y.J.; Won, J.; Park, N.-G.; Kang, Y.S. Dye-sensitized nanocrystalline solar cells based on composite polymer electrolytes containing fumed silica nanoparticles. *Chem. Commun.* **2004**, 1662. [[CrossRef](#)] [[PubMed](#)]
7. Wu, J.H.; Hao, S.C.; Lan, Z.; Lin, J.M.; Huang, M.L.; Huang, Y.F.; Fang, L.Q.; Yin, S.; Sato, T. A Thermoplastic gel electrolyte for stable quasi-solid-state dye-sensitized solar cells. *Adv. Funct. Mater.* **2007**, *17*, 2645. [[CrossRef](#)]
8. Wang, P.; Zakeeruddin, S.M.; Moser, J.E.; Nazeeruddin, M.K.; Sekiguchi, T.; Grätzel, M. A stable quasi-solid-state dye-sensitized solar cell with an amphiphilic ruthenium sensitizer and polymer gel electrolyte. *Nat. Mat.* **2003**, *2*, 402. [[CrossRef](#)]
9. Hayamizu, K.; Aihara, Y.; Arai, S.; Price, W.S. Diffusion, conductivity and DSC studies of a polymer gel electrolyte composed of cross-linked PEO, g-butyrolactone and LiBF₄. *Solid State Ion.* **1998**, *107*, 1–12. [[CrossRef](#)]
10. Kuila, T.; Acharya, H.; Srivastava, S.K.; Samantaray, B.K.; Kureti, S. Enhancing the ionic conductivity of PEO based plasticized composite polymer electrolyte by LaMnO₃ nanofiller. *Mater. Sci. Eng. B Solid State Mater. Adv. Technol.* **2007**, *137*, 217. [[CrossRef](#)]
11. Park, J.T.; Ahn, S.H.; Roh, D.K.; Lee, C.S.; Kim, J.H. Multifunctional organized mesoporous tin oxide films templated by graft copolymers for dye-sensitized solar cells. *ChemSusChem* **2014**, *7*, 2037. [[CrossRef](#)]
12. Yang, H.; Huang, M.; Wu, J.; Lan, Z.; Hao, S.; Lin, J. The polymer gel electrolyte based on poly(methyl methacrylate) and its application in quasi-solid-state dye-sensitized solar cells. *Mater. Chem. Phys.* **2008**, *110*, 38. [[CrossRef](#)]
13. Lim, S.M.; Moon, J.; Choi, G.H.; Baek, U.C.; Lim, J.M.; Park, J.T.; Kim, J.H. Surface carbon shell-functionalized ZrO₂ as nanofiller in polymer gel electrolyte-based dye-sensitized solar cells. *Nanomaterials* **2019**, *9*, 1418. [[CrossRef](#)]
14. Yoon, I.-N.; Song, H.; Won, J.; Kang, Y.S. Shape dependence of SiO₂ nanomaterials in a quasi-solid electrolyte for application in dye-sensitized solar cells. *J. Phys. Chem. C* **2014**, *118*, 3918. [[CrossRef](#)]
15. Zebardastan, N.; Khanmirzaei, M.H.; Ramesh, S.; Ramesh, K. Novel poly(vinylidene fluoride-co-hexafluoro propylene)/polyethylene oxide based gel polymer electrolyte containing fumed silica (SiO₂) nanofiller for high performance dye-sensitized solar cell. *Electrochim. Acta* **2016**, *220*, 573. [[CrossRef](#)]
16. Chae, H.; Song, D.; Lee, Y.-G.; Son, T.; Cho, W.; Pyun, Y.B.; Kim, T.-Y.; Lee, J.H.; Fabregat-Santiago, F.; Bisquert, J.; et al. Chemical effects of tin oxide nanoparticles in polymer electrolytes-based dye-sensitized solar cells. *J. Phys. Chem. C* **2014**, *118*, 16510. [[CrossRef](#)]
17. Sivakumar, R.; Akila, K.; Anandan, S. New type of inorganic-organic hybrid (heteropolytungstic acid–polyepichlorohydrin) polymer electrolyte with TiO₂ nanofiller for solid state dye sensitized solar cells. *Curr. Appl. Phys.* **2010**, *10*, 1255. [[CrossRef](#)]
18. Wiczorek, W. Composite polyether based solid electrolytes. The Lewis acid-base approach. *Solid State Ion.* **1996**, *85*, 67. [[CrossRef](#)]
19. Moon, J.; Shin, W.; Park, J.T.; Jang, H. Solid-state solar energy conversion from WO₃ nano and microstructures with charge transportation and light-scattering characteristics. *Nanomaterials* **2019**, *9*, 1797. [[CrossRef](#)]
20. Wagemaker, M.; Kearley, G.J.; van Well, A.A.; Mutka, H.; Mulder, F.M. Multiple Li positions inside oxygen octahedra in lithiated TiO₂ anatase. *J. Am. Chem. Soc.* **2003**, *125*, 840. [[CrossRef](#)] [[PubMed](#)]
21. Zhai, T.; Fang, X.; Liao, M.; Xu, X.; Zeng, H.; Yoshio, B.; Golberg, D. A comprehensive review of one-dimensional metal-oxide nanostructure photodetectors. *Sensors* **2009**, *9*, 6504. [[CrossRef](#)] [[PubMed](#)]
22. Devan, R.S.; Patil, R.A.; Lin, J.-H.; Ma, Y.-R. One-dimensional metal-oxide nanostructures: Recent developments in synthesis, characterization, and applications. *Adv. Funct. Mater.* **2014**, *22*, 3326. [[CrossRef](#)]

23. Ibrahim, I.; Lim, H.N.; Wan, N.W.K.; Huang, N.M.; Lim, S.P.; Busayaporn, W.; Nakajima, H. Plasmonic silver sandwich structured photoanode and reflective counter electrode enhancing power conversion efficiency of dye-sensitized solar cell. *Sol. Energy* **2021**, *215*, 403. [[CrossRef](#)]
24. He, Y.; Wang, W. ZIF-8 and three-dimensional graphene network assisted DSSCs with high performances. *J. Solid State Chem.* **2021**, *296*, 121992. [[CrossRef](#)]
25. He, G.; Wang, P.; Feng, K.; Dong, H.; Zhao, H.; Sun, F.; Yin, H.; Li, W.; Li, G. Efficient fabrication of diverse mesostructured materials from the self-assembly of pyrrole-containing block copolymers and their confined chemical transformation. *Macromolecules* **2021**, *54*, 906. [[CrossRef](#)]
26. Park, J.T.; Patel, R.; Jeon, H.; Kim, D.J.; Shin, J.-S.; Kim, J.H. Facile fabrication of vertically aligned TiO₂ nanorods with high density and rutile/anatase phases on transparent conducting glasses: High efficiency dye-sensitized solar cells. *J. Mat. Chem.* **2012**, *22*, 6131. [[CrossRef](#)]
27. Choi, G.H.; Kim, D.J.; Moon, J.; Kim, J.H.; Park, J.T. High-order diffraction grating as light harvesters for solar energy conversion. *J. Electroanal. Chem.* **2020**, *873*, 114490. [[CrossRef](#)]
28. Lee, J.Y.; Choi, G.H.; Moon, J.; Chi, W.S.; Park, J.T. 1D Co₄S₃ nanoneedle array with mesoporous carbon derived from double comb copolymer as an efficient solar conversion catalyst. *Appl. Surf. Sci.* **2021**, *535*, 147637. [[CrossRef](#)]
29. Kim, Y.E.; Baek, U.C.; Kim, J.H.; Chi, W.S.; Park, J.T. Harnessing SnO₂ nanotube light scattering cluster to improve energy conversion efficiency assisted by high reflectance. *Mater. Chem. Phys.* **2020**, *254*, 123538. [[CrossRef](#)]
30. Svanberg, C.; Adebahr, J.; Ericson, H. Diffusive and segmental dynamics in polymer gel electrolytes. *J. Chem. Phys.* **1999**, *111*, 11216. [[CrossRef](#)]
31. Aziz, S.B.; Woo, T.J.; Kadir, M.F.Z.; Ahmed, H.M. A conceptual review on polymer electrolytes and ion transport models. *J. Sci.* **2018**, *3*, 1. [[CrossRef](#)]
32. Kim, H.; Yang, B.L. Effect of seed layers on TiO₂ nanorod growth on FTO for solar hydrogen generation. *Int. J. Hydrog. Energy* **2015**, *40*, 5807. [[CrossRef](#)]
33. Zhao, Y.; Zhai, J.; Wei, T.X.; Jiang, L.; Zhu, D.B. Enhanced photoelectrical performance of TiO₂ electrodes integrated with microtube-network structures. *J. Mater. Chem.* **2007**, *17*, 5084. [[CrossRef](#)]
34. Tiwana, P.; Docampo, P.; Johnston, M.B.; Snaith, H.J.; Herz, L.M. Electron mobility and injection dynamics in mesoporous ZnO, SnO₂, and TiO₂ films used in dye-sensitized solar cells. *ACS Nano* **2011**, *5*, 5158. [[CrossRef](#)] [[PubMed](#)]
35. Park, J.T.; Chi, W.S.; Jeon, H.; Kim, J.H. Improved electron transfer and plasmonic effect in dye-sensitized solar cells with bi-functional Nb-doped TiO₂/Ag ternary nanostructures. *Nanoscale* **2014**, *6*, 2718. [[CrossRef](#)]
36. Karakuş, M.Ö.; Yakışıklar, M.E.; Delibaş, A.; Ayyıldız, E.; Çetin, H. Anionic and cationic polymer-based quasi-solid-state dye-sensitized solarcell with poly(aniline) counter electrode. *Sol. Energy* **2020**, *195*, 565. [[CrossRef](#)]
37. Kumar, S.; Manikandan, V.S.; Panda, S.K.; Senanayak, S.P.; Palai, A.K. Probing synergistic outcome of graphene derivatives in solid-state polymer electrolyte and Pt-free counter electrode on photovoltaic performances. *Sol. Energy* **2020**, *208*, 949. [[CrossRef](#)]
38. Mohan, K.; Bora, A.; Roy, R.S.; Nath, B.C.; Dolui, S.K. Polyaniline nanotube/reduced graphene oxide aerogel as efficient counterelectrode for quasi solid state dye sensitized solar cell. *Sol. Energy* **2019**, *186*, 360. [[CrossRef](#)]
39. Utomo, D.S.; Kim, J.H.; Lee, D.; Park, J.; Kang, Y.-C.; Kim, Y.H.; Choi, J.W.; Song, M. Fractional structured molybdenum oxide catalyst as counter electrodes of all-solid-state fiber dye-sensitized solar cells. *J. Colloid Interface Sci.* **2021**, *584*, 520. [[CrossRef](#)]
40. Xia, J.; Wang, Q.; Chen, M.; Li, W.; Liu, J.; Chen, J.; Wu, H.; Fan, S. Bifacial quasi-solid-state dye-sensitized solar cell with metal selenide M_{0.85}Se (M = Co, Ni) as counter electrode. *Electrochim. Acta* **2019**, *307*, 422. [[CrossRef](#)]
41. Yoo, B.; Kim, K.; Lee, D.-K.; Ko, M.J.; Lee, H.; Kim, Y.H.; Kim, W.M.; Park, N.-G. Enhanced charge collection efficiency by thin-TiO₂-film deposition on FTO-coated ITO conductive oxide in dye-sensitized solar cells. *J. Mater. Chem.* **2010**, *20*, 4392. [[CrossRef](#)]